



## OPTIMIZATION OF DUAL-EXPANDER ROCKET ENGINES IN SINGLE-STAGE-TO-ORBIT VEHICLES

Detlef Manski, Gerald Hagemann and Hagen D. Saßnick

Deutsche Forschungsanstalt für Luft- und Raumfahrt DLR

Lampoldshausen Research Centre

Space Propulsion Division

D-74239 Hardthausen a.K., Germany

### 1. Abstract

Dual-expander rocket engines offer a trajectory adapted dual-mode operation during the ascent of a launcher, which may be of significant advantage for single-stage earth-to-orbit vehicles, when compared to conventional rocket engines with bell-type nozzles.

This paper investigates a reusable single-stage earth-to-orbit vehicle with a constant payload capability of 16.5 Mg into low earth orbit, for the comparison of the dual-expander rocket engines with conventional rocket engines, using only hydrogen and oxygen as propellant combination in all engines.

Published by Elsevier Science Ltd.

### 2. Nomenclature

#### 2.1 Symbols

|                |                          |
|----------------|--------------------------|
| $A$            | area                     |
| $F$            | thrust                   |
| $g_0$          | normal earth gravitation |
| $I$            | impulse                  |
| $\dot{m}$      | mass flow                |
| $M$            | Mach number              |
| $p$            | pressure                 |
| $r$            | radius                   |
| $\Gamma_{O/F}$ | mass flow ratio ox/fu    |
| $T$            | temperature              |
| $t$            | time                     |
| $v$            | velocity                 |
| $\alpha$       | angle of attack          |
| $\Delta$       | difference               |
| $\epsilon$     | area ratio               |

#### 2.2 Subscripts

|        |                                      |
|--------|--------------------------------------|
| $c$    | combustion chamber                   |
| $comb$ | combustion                           |
| $div$  | divergence, multidimensional effects |
| $e$    | exit                                 |
| $eff$  | effective                            |
| $ine$  | inertial                             |
| $kine$ | kinetic                              |
| $fu$   | fuel                                 |
| $fric$ | friction                             |
| $grav$ | gravitation                          |
| $hl$   | heat loss                            |
| $mix$  | mixing, mixing point                 |
| $ox$   | oxidizer                             |

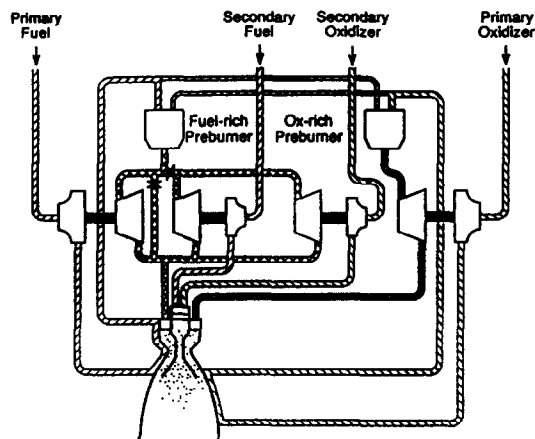


Figure 1: Full-flow dual-expander cycle with oxidizer- and fuel-rich preburners

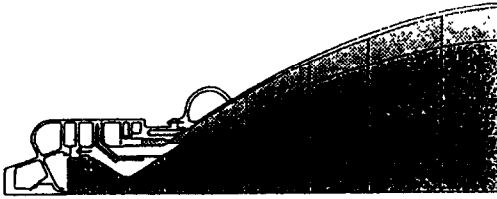
|          |                    |
|----------|--------------------|
| $r$      | ratio              |
| $s$      | specific           |
| $tot$    | total              |
| $vac$    | vacuum             |
| $vap$    | vaporization       |
| $pri$    | primary            |
| $rel$    | relative           |
| $sec$    | secondary          |
| $\delta$ | nominal propellant |

#### 2.3 Abbreviations

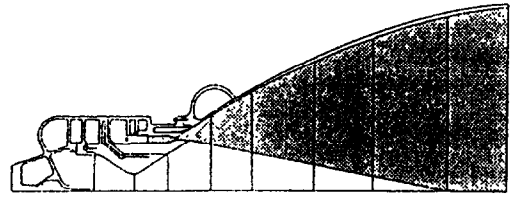
|      |                                 |
|------|---------------------------------|
| LEO  | low earth orbit                 |
| ODE  | one-dimensional equilibrium     |
| SSTO | Single-Stage-To-Orbit           |
| ST   | System Analysis Rocket Launcher |
| TSTO | Two-Stage-To-Orbit              |
| SSME | Space Shuttle Main Engine       |

### 3. Introduction and Literature Review

A single-stage-to-orbit vertical-takeoff and landing mission was applied to find out the potential advantage of full-flow dual-expander cycle engines versus conventional staged combustion engines. For the latter, two different staged combustion engines cycles were examined. Any advantage of mixed-mode



Mode 1 operation



Mode 2 operation

Figure 2: Dual-expander cycle mode 1 and 2 operations, following *Beichel* [2]

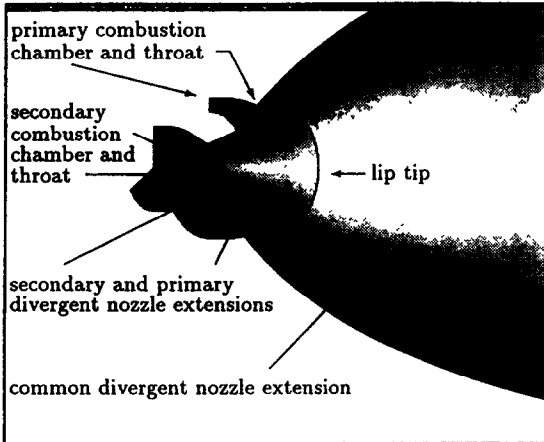


Figure 3: Sketch of dual-expander thrust chamber, cut-away view of combustion chambers and nozzles

propulsion could best be shown with single-stage-to-orbit vehicles, because these vehicles are the most sensitive launchers with regard to performance and mass.

Dual-expander engines for future launcher applications using one or two fuels and oxygen as oxidizer were suggested by *Beichel* [1]. The concept of this engine involves the use of a dense propellant combination with moderate performance during lift-off to provide high thrust for the initial flight phase, and a lower density, but better performing propellant combination in vacuum with a high specific impulse to reach the desired orbit velocity. Figure 1 explains the principle of the dual-expander cycle [3], and Fig. 2 shows the two operation modes, following *Beichel* [2]. In addition, Fig. 3 gives a cut-away view of both combustion chambers and the nozzle extensions. Several analytical works on SSTO- and TSTO vehicles using hydrogen/propane [2], [4], [5], [6] or hydrogen/methane [6], [7] as fuels revealed lowest vehicle dry masses for dual-expander engines in comparison to other engines. Thus, the better ranking of dual-expander engines using different fuels is well known.

Other dual-expander engines with hydrogen as a single fuel, but with dual mixture ratios [5], [8], [9] also revealed some benefits over conventional engines for SSTO- and TSTO applications. Despite of this, earlier investigations by the authors [4] have led to the results that dual-expander engines with hydrogen as single fuel compared with the conventional staged com-

bustion engine have no positive or, in some cases, even negative effects on payload delivery or dry mass reduction on advanced shuttles. The main reason for this result is that the mass of a dual-expander engine is larger than that of a conventional engine under the constraint of using the same number of engines for the launchers. In order to get a more reliable comparison, a further analysis was initiated taking into account all the additional advantages of the dual-expander engine. In this analysis the optimization of the dual-expander engine for single-stage-to-orbit vehicles and the comparison with different staged combustion cycle engines comprises the following items:

- using CFD-calculations to estimate the higher specific impulse losses of dual-expander nozzles, for the comparison with conventional engine nozzles [10], [11],
- varying additional parameters in contrast to earlier investigations [6], [10] for a fair comparison. This comprises also the number of engines.
- Taking the benefit of the cycle immanent thrust reduction capability of dual-expander engine for the comparative analysis, and a
- complete redesign of the dual-expander engine cycle shown in Fig. 1.

Due to time restrictions, the last two items are not treated in full detail in this paper.

#### 4. System Analysis Programme ST

To analyse various kinds of rocket engine cycles for future space transportation systems, a propulsion system analysis programme ST has been developed which contains both DLR and NASA developed methods, see [12], [13], [14], [15], [16] for further details. The programme consists of several routines carrying out engine performance calculations [17], [18], engine system power matching calculations, engine mass calculations, vehicle mass calculations, vehicle performance calculations and trajectory calculations [21]. By using ST, many vehicle parameter are to be determined to fulfill the given conditions, such as payload mass, engine type, propellant combination.

## 5. Reference vehicle

A single-stage-to-orbit vertical-takeoff and landing vehicle was chosen for this comparative cycle analysis. The vehicle is of BETA- or Delta-Clipper-type, following proposals by [19] and [20] and a re-examination by [6]. In contrast to the proposal [19], in this analysis the number of dual-expander engines integrated in the SSTO launcher is assumed to be half of the corresponding numbers of conventional engines for better comparison purpose, because each dual-expander engine has a duplication of components such as nozzles, chamber, turbopumps etc.. Thus, eight engines were used in case of the staged combustion cycles and 4 engines in case of the full-flow dual-expander cycle. Arrangement of the engines are shown in Figure 4, viewing on the scaled nozzle exit areas at the base.

Thrust reduction by this arrangement for the staged combustion engines will be performed at a predefined value for the maximum allowable acceleration by shutting down two engines located opposite to each other, which can occur up to three times.

The dual-expander engine has a build-in acceleration reduction capability, achieved by shutting down the secondary inner flow. The total engine thrust will then be provided only by the outer or primary flow which uses the total nozzle exit area, leading to an increase in specific impulse. This shut-down of the secondary flow is determined by the stage parameter mass ratio  $m_r$ ,

$$m_r = \frac{m_{s_{pri}}}{m_{s_{pri}} + m_{s_{sec}}}, \quad (1)$$

and the propulsion parameter thrust ratio  $F_r$ ,

$$F_r = \frac{F_{pri}}{F_{pri} + F_{sec}}. \quad (2)$$

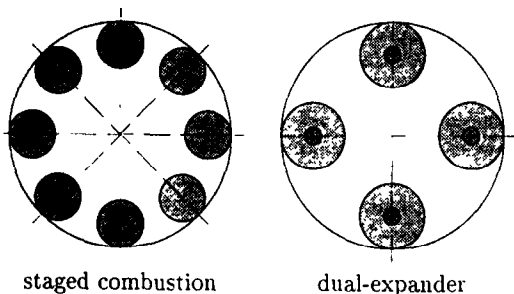


Figure 4: Sketch of launch vehicle base showing the arrangement of engines

In this paper, a constant  $3-g_0$ -limit in the trajectory calculations was assumed for the vehicles with staged combustion cycles. For vehicles powered by dual-expander cycles, an acceleration decrease occurs at switch-over from mode 1 to mode 2 operation.

The following assumptions for the vehicle model were taken into consideration:

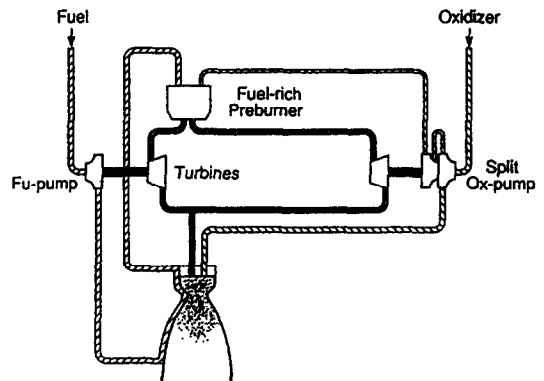


Figure 5: Staged combustion cycle with fuel-rich preburner and split oxidizer pump

### 5.1 Vehicle model

- Using ST-vehicle mass model [15],
- 6 landing gears,
- cylindrical tank, diameter 8 m, elliptical endcaps with an ellipse ratio of 1.5,
- main propellants and extra tanks for reentry, orbit control and reserves,
- constant payload of 16.5 tons into a 200 km circular orbit from French Guyana, Kourou, following an ESA requirement,
- constant payload fairing of 2.6 tons until injection, and an
- acceleration limit  $3-g_0$ .

Additionally, the following assumptions for the propulsion model were considered:

### 5.2 Propulsion model

- Using ST-performance, cycle and engine mass model [16].
- hydrogen-rich preburner mixture ratio 0.85:1.
- oxygen-rich preburner mixture ratio 100:1,
- isentropic efficiencies for all turbines and pumps at 75 %,
- pressurants, helium for oxygen, hydrogen for hydrogen,
- constant  $\eta_{c^*}$  efficiency of 99 %,
- nozzle efficiencies taken from CFD-calculations.

## 6. Cycles for comparative analysis

For comparison with the advanced dual-expander engine cycle, the mono mode staged combustion cycle will be used, which has the highest performance of all mono mode rocket engines. The expansion of all propellants from a high chamber pressure makes it

possible to attain high overall specific impulses. However, the staged combustion cycle has a maximum attainable chamber pressure. This pressure depends on the staged combustion subcycle type, on the allowable temperature in the preburner, on the efficiencies of turbines and pumps, and on the injector pressure ratio needed for a stable and efficient combustion. Several types of staged combustion subcycles are considered in ST. The following staged combustion cycles of ST are chosen for this comparison:

1. The staged combustion cycle with one fuel-rich preburner and an oxidizer split pump, as plotted in Figure 5.
2. The simple full-flow staged combustion cycle with complete preburning using two oxidizer- and fuel-rich preburners, which is plotted in Figure 6.

This simple full-flow staged combustion cycle is more suited for a fair comparative analysis with the dual-expander cycle used in this paper, due to the lack in the ST-analysis of a simpler dual-expander cycle using only fuel-rich preburners.

The highest chamber pressure for a staged combustion cycle can be reached with the full-flow staged combustion cycle with complete oxidizer- and fuel-rich preburning, and an auxiliary pump for matching preburner exit pressures. This engine cycle is shown in Figure 7.

Within this comparative study, it is not necessary to include this cycle, because the system optimum chamber pressures lie far below the significantly higher chamber pressures which are achievable with this cycle [4]. Thus, the simple full-flow staged combustion cycle shown in Fig. 6 delivers sufficient high chamber pressures for an optimum SSTO vehicle powered by conventional engines.

### 7. Optimization

The optimizations were made under the condition of a constant payload into a circular low earth orbit of 200

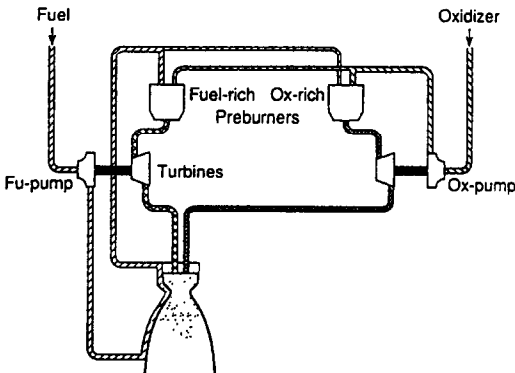


Figure 6: Simple full-flow staged combustion cycle with oxidizer- and fuel-rich preburners

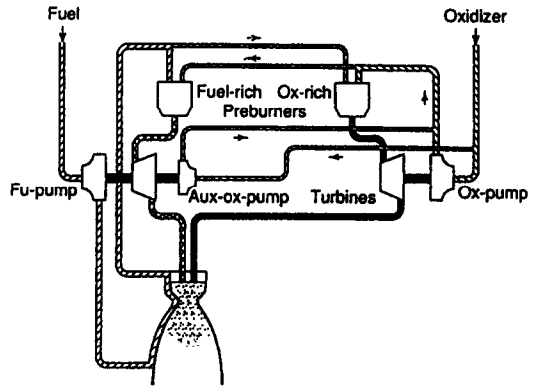


Figure 7: Full-flow staged combustion cycle with oxidizer- and fuel-rich preburners and auxiliary pump for matching preburners exit pressures

km altitude by minimizing the effective net mass of the single stage vehicle. A low structure and engine mass is one of the criteria for a cost-minimized launcher system. The optimizations were made versus the design propulsion parameters, chamber pressure and mixture ratio. The propellant combination chosen is hydrogen and oxygen. A minimization of net mass is done for all three engine cycles, the staged combustion cycle with fuel-rich preburner and split oxidizer pump, the simple full-flow staged combustion, and the full-flow dual expander cycle.

### 8. Trajectory Calculations

Trajectory calculations were made using POST [21]. In order to optimize the SSTO vehicle as function of different propulsion and stage parameters, the ST mass- and performance models are used to iterate the launcher for the given constant payload. For this iteration, a total velocity requirement  $\Delta v_{tot}$  is estimated. The calculated masses and performance data are then used in the trajectory optimization, which delivers the exact required  $\Delta v_{tot}$ . This modified value of  $\Delta v_{tot}$  serves as reference value in a second iteration of the launcher using again the ST mass and performance models. This coupling of the mass- and performance models with the trajectory optimization requires an iterative procedure, but many test runs have demonstrated that the second trajectory iteration loop will not substantially change the results or tendencies so that generally one trajectory iteration loop is sufficient.

The manoeuvres and events of a launch sequence chosen for the optimization of the trajectories of the SSTO vehicles are summarized in Table 1.

### 9. Results of CFD-analyses of dual-expander nozzles

For the optimization calculations performed with the ST programme, the expansion of the flow in the

| Phase | Event                       | Events description  |
|-------|-----------------------------|---|
| 1     | 0 - 12 s                    | Vertical ascent   |
| 2     | 12 - 22 s                   | Pitch manoeuvre at constant inertial pitch rate and constant azimuth of the launch-centered inertial co-ordinate system. The pitch rate and azimuth are subject to optimization.  |
|       | roving                      | If secondary propellants are burned out, the primary flow continuously burns under reduced thrust and higher specific impulse by adapting the total nozzle exit area as expansion area ratio                                      |
| 3     | 22 s - $t_{\alpha=0^\circ}$ | Flight with constant inertial pitch angle till zero angle of attack in the pitch plane is reached.  |
| 4     | $H = 30$ km                 | Gravity turn where the angle of attack remains zero and the trajectory is curved due to the gravity fields of the Earth till an altitude of 30 km is reached.   |
| 5     | $\Delta t = 0.5$ s          | Inertial body rate initialization using the inertial pitch angle. The pitch angle is subject to optimization.   |
| 6     | $v_{rel} = 1500$ m/s        | Piecewise linear steering till the desired inertial pitch angle and velocity at the end of this phase is reached. The pitch angle is subject to optimization.   |
| 7     | $v_{rel} = 3000$ m/s        | same as above   |
| 8     | $v_{rel} = 4000$ m/s        | same as above   |
| 9     | $v_{ine} = 5000$ m/s        | same as above   |
| 10    | $v_{ine} = 7784$ m/s        | Piecewise linear steering during the remaining flight time till injection into the final orbit is reached at altitude 200 km and by a flight path angle to inertial velocity of zero. The pitch angle is subject to optimization. |

Table 1: Sequence of events for the SSTO trajectory into LEO

|   | Mode 1 (prim./sec.) | Mode 2  |
|---|---------------------|---------|
| chamber pressure $p_c$                                | 200 / 200 bar       | 200 bar |
| mixture ratio $r_{O/F}$                               | 7 / 7               | 7       |
| primary nozzle throat radius                          | .10418 m            |         |
| ratio of throat areas, $A_{t,pr}/A_{t,sec}$           | 1.                  |         |
| nozzle exit area ratio $\epsilon$                     | 58. / 58.           | 116.    |
| area ratio mixing primary flow $\epsilon_{pr,mix}$    | 5.                  | -       |
| area ratio mixing secondary flow $\epsilon_{sec,mix}$ | 5.                  | -       |

Table 2: Dual-expander engine design data used for CFD-analysis [10]

|                          | dual-expander nozzle   |   |                              | conventional nozzle<br>(staged-combustion<br>cycle) |
|--------------------------|------------------------|---|------------------------------|---|
|                          | Mode 1<br>(prim./sec.) | Mode 2, with<br>bleed gas<br>(prim./sec.) | Mode 2. without<br>bleed gas |   |
| chamber pressure $p_c$   | 200 / 200 bar          | 5 / 200 bar                               | 200 bar                      | 200 bar   |
| mixture ratio $r_{O/F}$  | 7 / 7                  | 7 / 7                                     | 7                            | 7   |
| kinetic loss             | 0.999                  |   |                              |   |
| friction loss            | 0.994                  | 0.991                                     | 0.991                        | 0.994   |
| divergence loss          | 0.984                  | 0.986                                     | 0.982                        | 0.990   |
| combustion loss $\eta_c$ | 0.990                  |   |                              |   |
| overall loss             | 0.967                  | 0.966                                     | 0.972                        | 0.973   |

Table 3: Summary of dual-expander flowfield analysis [10], [22]

nozzles is simulated with the assumption of one-dimensional, inviscid flow in chemical equilibrium. Losses due to non-complete mixing and burning, friction, chemical non-equilibrium effects, and multi-dimensional flow effects are taken into account by loss efficiencies in the final impulse balance. Following the JANNAF Performance Methodology [11], [22], the specific impulse can then be determined from:

$$I_{s,eff} = (\eta_{I_{comb}} \cdot \eta_{I_{mix}} \cdot \eta_{I_{exp}} \cdot \eta_{I_{kin}} \cdot \eta_{I_{div}} \cdot \eta_{I_{fric}} \cdot \eta_{I_{hl}}) I_{s,ODE} \quad (3)$$

The first three efficiencies are summarized to give the efficiency of energy release in the combustion chamber, which is assumed to be  $\eta_c = 0.99$  in all of the analyses presented in this paper. Heat losses across nozzle walls, *hl*, i.e. by regenerative cooling, are considered and included in the boundary layer losses, *fric*, and therefore characterized by  $\eta_{I_{fric}}$  [11].

For conventional nozzles, a large data base of these loss efficiencies as a function of characteristic nozzle design parameters exists [11], [22]. Due to lack of data for advanced rocket nozzles, CFD-analyses of dual-expander nozzles were performed. These analyses were based on a dual-expander engine suggested in [4], for a winged SSTO vehicle delivering 13.5 Mg payload into LEO. The propulsion design data are given in Table 2, further details on the launcher design are given in [4], [10]. Table 3 summarizes the main findings of the numerical simulations for the dual-expander nozzles. The CFD-analysis of the mode 1 operation revealed compression- and shock wave formations in the nozzle, which are induced due to the inhomogeneous pressure distribution in the cross section, where the exhaust gases of the primary and secondary combustion chamber are mixed.

The numerical simulation of the mode 2 operation revealed a transient flow behaviour in the inner chamber. To avoid all non-stationary effects in the inner chamber, which may cause structural failures of the hardware, an alternative mode 2 operation was proposed, where bleed gas is injected into the inner chamber at moderate chamber pressures.

Despite of the shock- and expansion waves in the nozzle, the calculated overall performance data of the investigated dual-expander nozzles indicate a high performance during both operation modes. Efficiencies for friction and the divergence of the flowfield are also given in Table 3, which will serve as reference values in the following engine analyses.

Corresponding efficiency values of a conventional SSME-type nozzle are also included in Table 3. Further details on the CFD-calculations and results are included in [10] and [22].

## 10. System parameter analysis

### 10.1 Efficiency sensitivity on SSTO vehicles

The efficiencies of conventional and dual-expander rocket nozzles, as summarized in Table 3, are very high. However, even a decrease in the nozzle efficiency by one permille leads to a significant increase in launcher take-off and effective net masses, as pointed out in Figure 8. In there, the effective net mass is plotted for all three cycles versus the specific impulse efficiency which contains both, the nozzle and the combustion chamber efficiency. Additional parameters kept constant in Figure 8 are the mixture ratio of 7:1, and the chamber pressure of 200 bar for all three cycles. The family of thin lined curves represents the first calculations performed with ST using the constant  $\Delta v_{tot}$  requirement of 9300 m/s. The coupling with the trajectory optimization leads to a decrease in slope of the net mass versus specific impulse efficiency. The slope of the dual-expander cycle engine is less compared to the simple staged combustion and full-flow staged combustion cycles.

The considered dual-expander cycle shows best performance with regard to minimum launcher net masses, although it has higher turbo-machinery weight as the full-flow staged combustion cycle. The advantage of the dual-expander cycle is based on the two operation modes which permits a better adaptation to the decreasing atmospheric pressure during the ascent of the SSTO launcher from sea level to vacuum. The parametric variation of the nozzle exit pressures, and thus of the nozzle exit area ratio, for the two modes of the dual-expander cycle and the one mode of the staged combustion cycle will be shown in the next chapter.

### 10.2 Nozzle exit pressure optimizations

The effective net mass versus the nozzle exit pressure of the staged combustion cycle is shown in Figure 9. The thin line curve family represents the results of the first calculations which were performed with an estimated  $\Delta v_{tot}$  kept constant for all cases. The thick line curve family represents the results received after the 1st trajectory iteration. It can be seen that the optimum nozzle exit pressure (that is the averaged value in the exit plane) will be reached at  $p_{e,ODE} = 0.3$  bar, which is far above the value given by the Summerfield criterion to avoid flow separation in the nozzle during take-off. This separation criterion leads to an averaged exit pressure of approx.  $p_{e,ODE} = 0.18$  bar [22].

This variation indicates, that the nozzle exit pressure of a single-stage-to-orbit vehicle must be lower than corresponding values of first stage nozzles of a simple multistage rocket, e.g of the Ariane 4. Only in case launch vehicles using thrust supporting solid boosters like the Ariane 5 and Space Shuttle, the nozzle exit pressures are even lower and equal to the separation criterion, a result of optimizations of these vehicles.

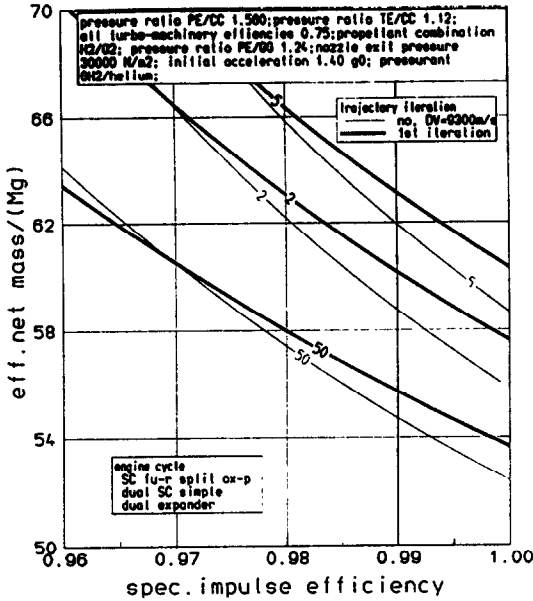


Figure 8: Sensitivity of SSTO vehicles versus specific impulse efficiency for different engine cycles, line 2: staged combustion cycle with fuel-rich preburner and split oxidizer pump (Fig. 5) line 5: simple full-flow staged combustion cycle (Fig. 6) line 50: full-flow dual-expander cycle (Fig. 1)

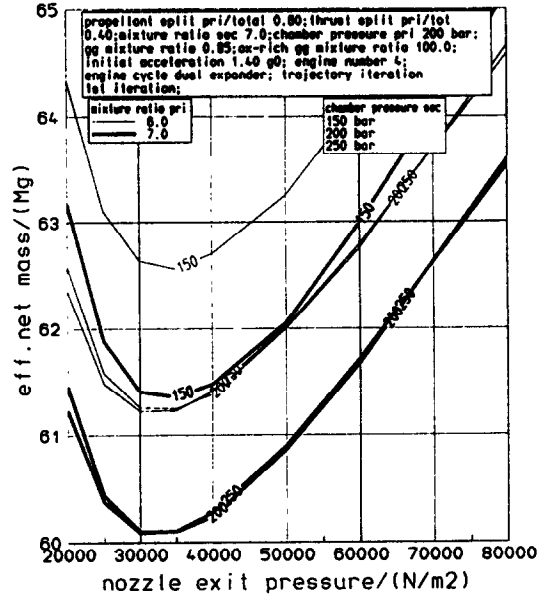


Figure 10: Optimization of nozzle exit pressure for dual-expander engine during low altitude operation, both combustion chambers active (mode 1)

seen in Figure 10. A higher nozzle exit pressure at sea level correlates with a lower nozzle extension ratio and, at the same time, with a lower specific impulse in vacuum. This is also adequate for the dual-expander engine, but the switch over from mode 1 to mode 2 operation leads to a significant higher nozzle expansion ratio than that of the comparable mono mode engines for high altitude and vacuum operation. The obtained nozzle exit area ratios of the dual-expander engines for the mode 2 operation in vacuum are shown later in this paper.

The variation of chamber pressure and mixture ratio has no influence on the nozzle exit pressure optimization, but on the effective net masses, as it can be seen in Fig. 10. Figure 11 shows the total velocity requirement for the nozzle exit pressure optimization for the dual-expander engine. Of course, the required  $\Delta v_{tot}$  is very sensitive on nozzle exit pressures, but it shows only minor influence on chamber pressures and mixture ratios.

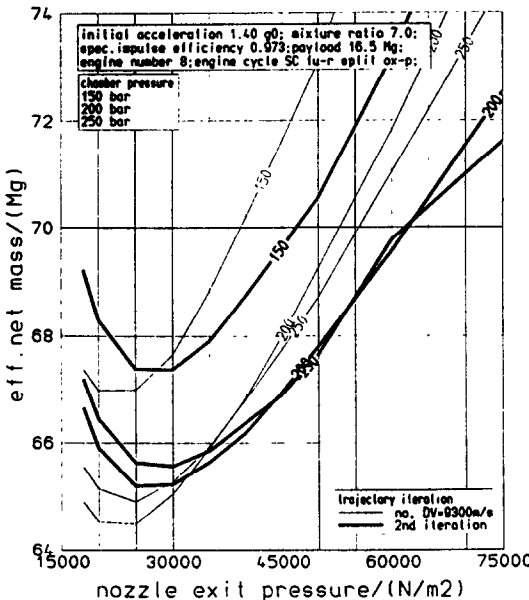


Figure 9: Optimization of nozzle exit pressure for mono mode cycles, staged combustion cycle with fuel-rich preburner and split oxidizer pump

It is surprising, that even the dual-expander cycle with its two modes also optimized at  $p_{e,ODE} = 0.3$  bar nozzle exit pressure during mode 1 operation, as it can be

### 10.3 Thrust level optimizations

Thrust level optimization is a trade-off between less gravitational losses  $\Delta v_{grav}$  versus higher effective net masses, caused by higher engine and thrust frame masses. Figure 12 shows the result of this trade-off. The optimum take-off acceleration for the vehicle with the eight staged combustion engines with fuel-rich preburners and split oxidizer pumps is very flat between  $1.3g_0$  and  $1.4g_0$ . As result, a take-off acceleration of  $1.4g_0$  is chosen for all further variations.

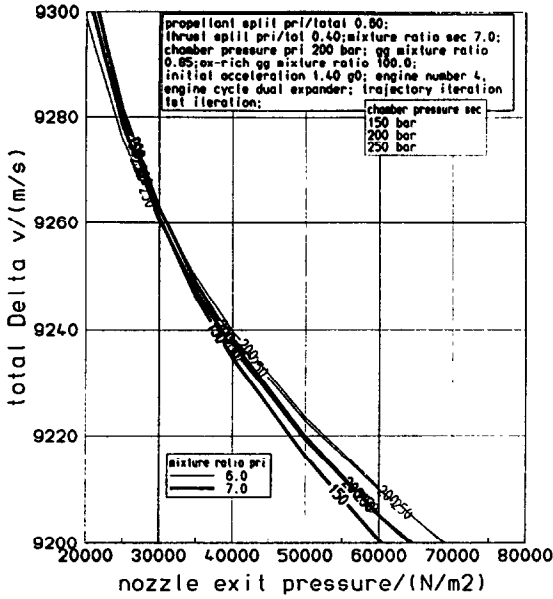


Figure 11: Total velocity requirement as function of the nozzle exit pressure for dual-expander engines, varying secondary chamber pressure and mixture ratio

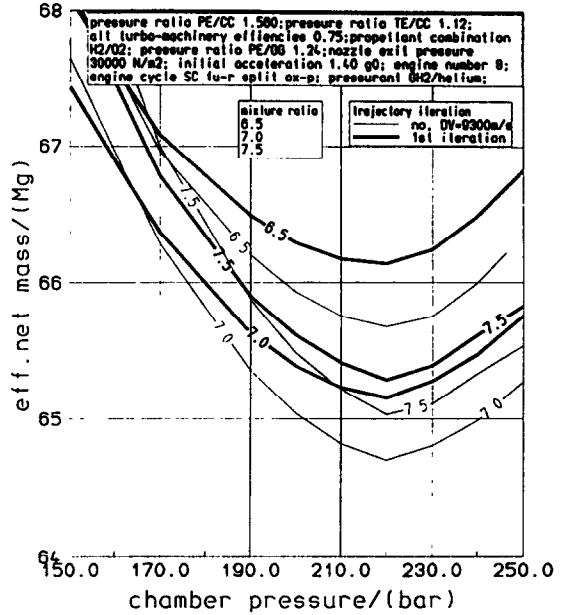


Figure 13: Chamber pressure optimization for the staged combustion cycle with fuel-rich preburner and split oxidizer pump

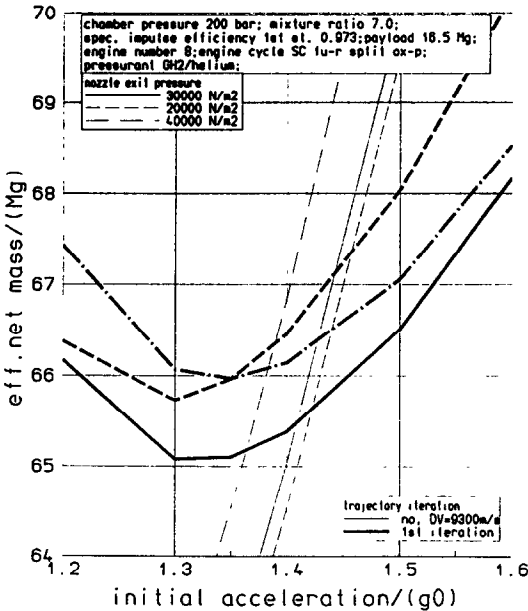


Figure 12: Optimization of take-off acceleration for the SSTO vehicle powered by the staged combustion cycle with fuel-rich preburner and split oxidizer pump

## 11. Payload delivering performance

### 11.1 Staged combustion cycle

The payload delivering performance of different SSTO vehicles will be shown by their effective net mass, which is needed to deliver the the same payload into

the same orbit. This point of view leads to cost effective launchers with minimum effective net masses. Figure 13 shows this relation for the variation of the rocket chamber pressure and mixture ratio for the staged combustion cycle with fuel-rich preburner and split oxidizer pump (Fig. 5). One can see that a minimum net mass will be reached at a relatively low chamber pressure of 220 bar, which is almost independent of the selected mixture ratios.

The relatively low optimum chamber pressure lying far below the maximum possible chamber pressure could be explained by the high growth of turbo-machinery mass when chamber pressure increases. Therefore, the effect of additional specific impulse increase is lower than that of the increased mass of the engine. For the analysis performed here, Space Shuttle technology for the turbo-machinery with isentropic turbo-pump efficiencies of 75% and a preburner temperature of about 900 K (preburner mixture ratio of 0.85) is assumed. For a higher turbo-pump technology, also for lightweight liquid rocket engines, the optimum chamber pressure will move up to higher values [4].

The optimization of the mixture ratio for oxygen and hydrogen for selected near optimum chamber pressures is shown in Figure 14. It can be seen, that the optimum mixture ratio is in a regime between 7-7.2, and at a chamber pressure of 220 bar. This is almost independent within the chamber pressure interval shown in Fig. 14, and for the trajectory iteration and constant  $\Delta v_{tot}$ -calculations.

The minimum structure mass is achieved at a mix-

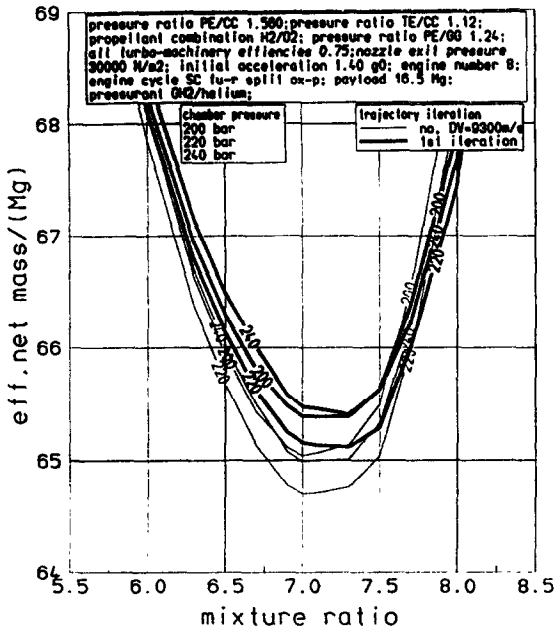


Figure 14: Mixture ratio optimization for the staged combustion cycle - mixture ratio vs. effective net mass

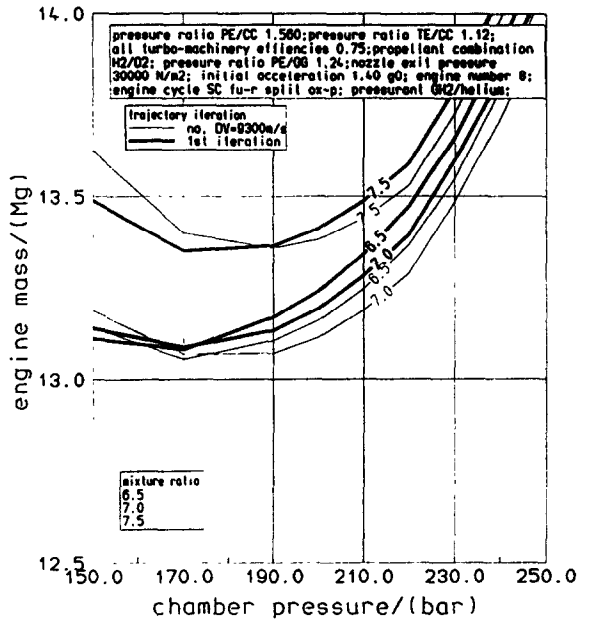


Figure 16: Chamber pressure optimization for the staged combustion cycle - chamber pressure vs. engine mass

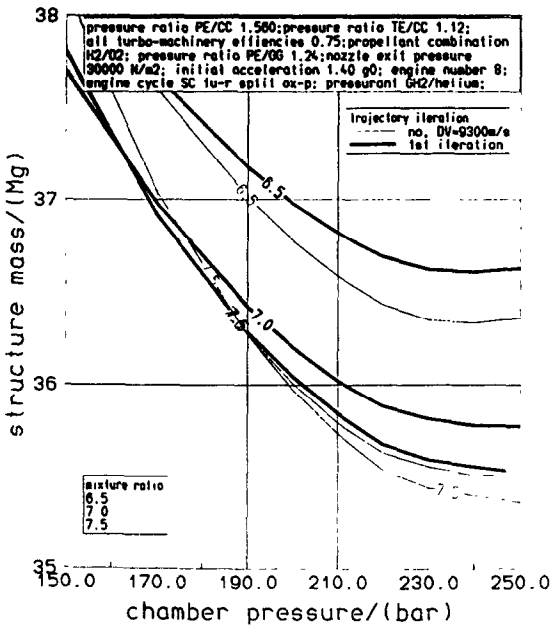


Figure 15: Chamber pressure optimization for the staged combustion cycle - chamber pressure vs. structure mass

ture ratio of 7.5 at 250 bar chamber pressure, see Fig. 15, and the minimum engine mass at 6.7 and 170 bar, shown in Fig. 16. These minimum structure and engine masses result in the previously indicated optimum for the effective net mass.

### 11.2 Full-flow staged combustion cycle

Figures 17 and 18 show the optimization of the chamber pressure and mixture ratio for the simple full-flow staged combustion cycle (Fig. 6).

Due to the relatively low optimum chamber pressure for SSTO vehicles it is obvious that the simple full-flow staged combustion cycle will present no advantages over the other cycles with regard to the payload performance of SSTO vehicles. This cycle has no higher specific impulses at the same chamber pressures than the other cycles, but needs higher turbo-machinery masses, which causes an increase in effective net masses of approx. 4 tonnes, compared with the staged combustion cycle with only one fuel-rich preburner. The simple full-flow staged combustion cycle may be suited if higher chamber pressures are applicable

### 11.3 Full-flow dual-expander cycle

Earlier optimizations by the authors using reusable winged vehicles [4] have lead to the result that the dual-expander engines using hydrogen and oxygen in both flows have an optimum nearby mixture ratios of 7/7 and chamber pressures of 200/200 in primary and secondary flows. Therefore, for this analysis only optimizations nearby that domain were investigated. Figure 19 shows at this domain a mass split rate and thrust split rate optimization (see Eq.(1) and Eq.(2)) for the dual-expander cycle. These two parameters strongly influence the trajectory, so that constant  $\Delta v$ -calculations are not applicable, as it can be seen in Fig. 19 by the thin line curve family. These results show.

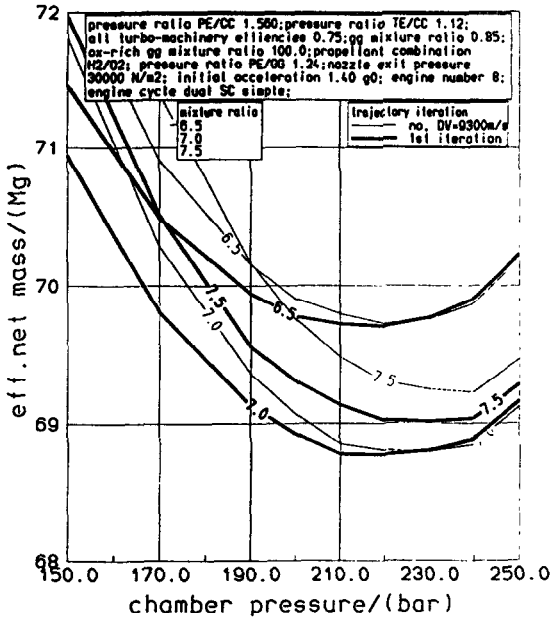


Figure 17: Chamber pressure optimization for the simple full-flow staged combustion cycle

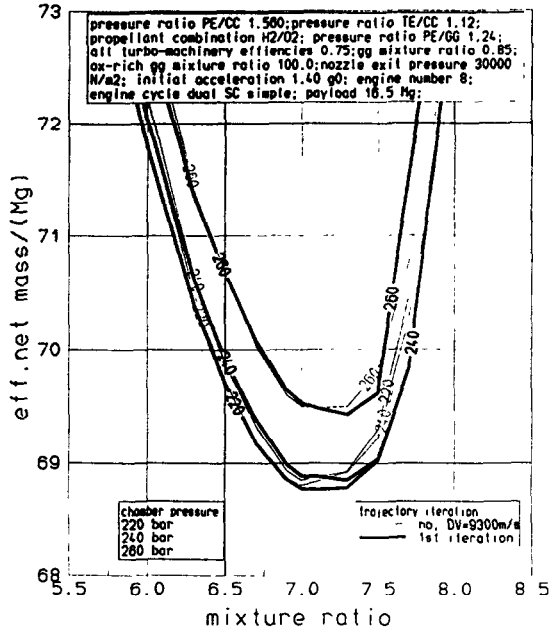


Figure 18: Mixture ratio optimization for the simple full-flow staged combustion cycle

that the lowest effective net mass for this cycle is 7 tonnes lower or 10 % below the effective net mass of the vehicle powered by the simple full-flow combustion engines, and it is reached at a thrust split rate of 0.4 and a mass split rate of 0.6.

In Fig. 19, the propellant mass split rate of 0.5 has the same low value, but it is placed near the cycle limit, and therefore might be not a good design point

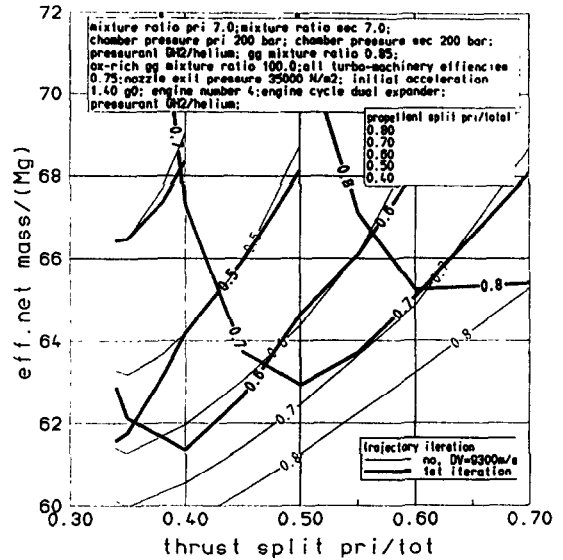


Figure 19: Thrust and mass split optimization of the dual-expander cycle at chamber pressures 200/200 bar and at mixture ratios 7/7

for this type of dual-expander cycle. This cycle limit is caused by the oxygen-rich preburner which cannot deliver enough energy to pump the propellants to the high primary chamber pressure of 200 bar. Because of the relatively low chamber pressure necessary for SSTO vehicles, a reduction in chamber pressures and a reduction in mixture ratios on the primary side seems to be an approach to reach lower stable thrust split rates for the mass split rates of 0.5 and below.

Figure 20 summarizes this search for an optimum nearby the design point of Fig. 19. This optimum is found at a primary chamber pressure of 150 bar and a secondary chamber pressure of 200 bar. The mixture ratio in the primary chamber is 6.5, and 7.5 in the secondary chamber. The value for the mass split rate is 0.45, and for the thrust split rate 0.26. This optimization was performed for a nozzle exit pressure of  $p_{eODE} = 0.35$  bar during the mode 1 operation, a result of the exit pressure optimization shown in Fig. 10. The corresponding nozzle exit area ratios during mode 2 operation in vacuum are shown in Fig. 21.

## 12. Summary of optimized engine cycles

Table 4 shows a summary of the most important system and performance data of the best candidates for each cycle investigated. The SSTO vehicle with full-flow dual-expander engines has the lowest effective net mass, compared to the vehicles equipped with the stage combustion cycles. The effective net mass relative to the propellant mass needed for the mission with a fixed payload is higher for the dual-expander engines, but the better performance during the ascent to orbit and the lower number of engines allow a more efficient construction, which makes this type of cycle

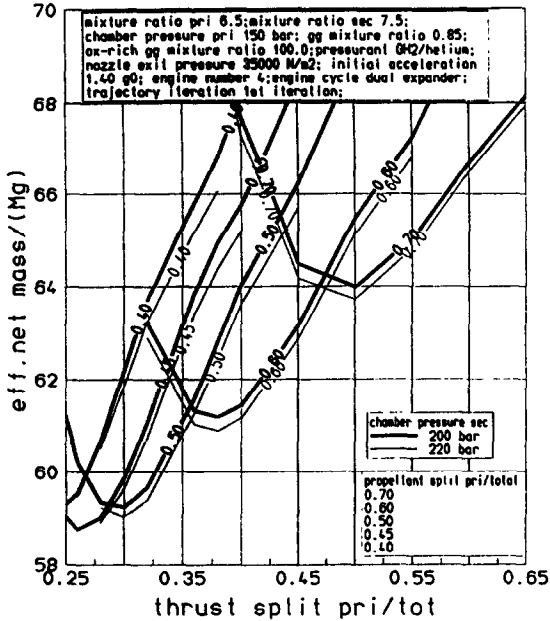


Figure 20: Thrust and mass split optimization of the dual-expander cycle at chamber pressures 150/200 and 150/220 bar and at mixture ratios 6.5/7.5

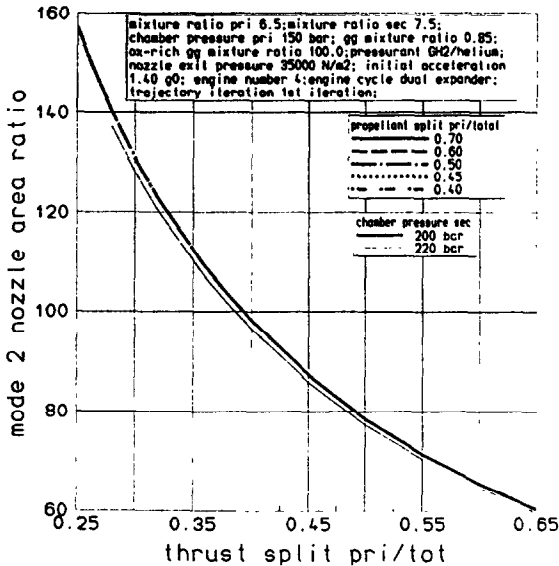


Figure 21: Nozzle exit area ratio for the mode 2 operation as function of thrust split for the dual-expander cycle at chamber pressures 150/200 and 150/220 bar and at mixture ratios 6.5/7.5

favorable.

To illustrate the components needed for the engine and structure mass, Table 5 shows a summary of the most important subsystem mass data of the best candidate for each cycle investigated. The engine subsystem data are given for a single engine. Because the number of engine are different for the cycles investi-

gated, the mass subsystem data are based on different thrust levels.

### 13. Conclusion

Using CFD-calculations and NASA and DLR developed software for system analysis it has been shown, that full-flow dual-expander engines with the propellants hydrogen/oxygen offer a wide performance increase, when applied in SSTO vehicles.

One reason for the high advantage of the dual-expander engines is the reduced engine number of four, instead of eight engines as used in earlier investigations. Thus, the launcher powered with the dual-expander engines has lowest overall engine masses, which also minimizes the launcher effective net masses.

The simple full-flow staged combustion cycle has less performance in SSTO vehicles than the staged combustion cycle with a fuel-rich preburner and a split oxidizer pump.

The results presented in this paper allow to prognosticate that a simple dual-expander engine with only fuel-rich preburner will deliver better performance in SSTO vehicle than the full-flow dual-expander engine, because of the low primary chamber pressures which are necessary for system optimizations of SSTO vehicles with dual-expander engines. Dual-expander engines with only one fuel-rich preburner could be pushed towards a higher primary chamber pressure after burn-out of the secondary, inner flow. This would give an additional increase in payload delivering performance against the full-flow dual-expander cycle.

### References

- [1] R. Beichel, *The Dual-expander Rocket Engine - Key to Economical Space Transportation*, Astro-nautics and Aeronautics, Vol. 15, No. 11. 1977
- [2] R. Beichel, C. J. O'Brian, J. P. Taylor, *The Next Generation Rocket Engines*, IAF-89-4219. 1988
- [3] H. Taniguchi, D. Manski, *Performance of Advanced Engine Cycles in Future Launcher Systems*. IAF-87-065, 1987
- [4] D. Manski, J. A. Martin, *Evaluation of Innovative Rocket Engines for Single-Stage Earth-to-Orbit Vehicles*, Journal of Propulsion and Power. Vol.7. No.6, Nov./Dec. 1991, pp. 929-937
- [5] J. A. Martin, D. Manski, *Variable Mixture Ratio and other Rocket Engines for Advanced Shuttles*. AIAA-89-2282, 1989
- [6] D. Manski, A. Fina, *Advanced Rocket Propulsion Systems for Reusable Ballistic SSTO Vehicles BETA & Delta-Chopper*, AIAA-94-3316. 1994
- [7] J. A. Martin, *Space Transportation Main Engines for Two-Stage Shuttles*. AIAA-88-2929. 1988

| variable                         | dual-<br>expander cycle | full-flow<br>staged comb. cycle | fuel-rich<br>staged comb. cycle | unit             |
|----------------------------------|-------------------------|---------------------------------|---------------------------------|------------------|
| propellant split pri/total       | .45                     | -                               | -                               |                  |
| thrust split pri/tot             | .26                     | -                               | -                               |                  |
| engine number                    | 4                       | 8                               | 8                               |                  |
| propellant combi. primary        | $H_2/O_2$               | $H_2/O_2$                       | $H_2/O_2$                       |                  |
| propellant combi. secondary      | $H_2/O_2$               | -                               | -                               |                  |
| pressurant                       | $H_2/He$                |                                 |                                 |                  |
| chamber pressure pri             | 150.                    | 220                             | 220                             | bar              |
| chamber pressure sec             | 200.                    | -                               | -                               | bar              |
| mixture ratio pri                | 6.5                     | 7                               | 7                               |                  |
| mixture ratio sec                | 7.5                     | -                               | -                               |                  |
| nozzle area ratio primary        | 39                      | 62                              | 62                              |                  |
| nozzle area ratio secondary      | 54                      | -                               | -                               |                  |
| mode 2 nozzle area ratio         | 151                     | -                               | -                               |                  |
| vacuum spec.impulse primary      | 4295                    | 4381                            | 4381                            | Ns/kg            |
| vacuum spec.impulse secondary    | 4288                    | -                               | -                               | Ns/kg            |
| sea level spec.impulse pri       | 3686                    | 3731                            | 3731                            | Ns/kg            |
| sea level spec.impulse sec       | 3678                    | -                               | -                               | Ns/kg            |
| mode 1 sea level Isp             | 3680                    | 3731                            | 3731                            | Ns/kg            |
| mode 2 vacuum Isp                | 4519                    | -                               | -                               | Ns/kg            |
| spec. impulse efficiency pri     | 0.967                   | 0.973                           | 0.973                           |                  |
| spec. impulse efficiency sec     | 0.966                   | -                               | -                               |                  |
| mode1 sea level thrust           | 2021.                   | 1183                            | 1136                            | kN               |
| mode2 vacuum thrust              | 644.                    | 1388                            | 1334                            | kN               |
| sea level thrust primary         | 526.                    | 1183                            | 1136                            | kN               |
| sea level thrust secondary       | 1496.                   | -                               | -                               | kN               |
| total sea level thrust           | 8086.                   | 9460                            | 9090                            | kN               |
| total vacuum thrust              | 9426.                   | 11107                           | 10672                           | kN               |
| payload                          | 16.5                    | 16.5                            | 16.5                            | Mg               |
| initial mass                     | 611                     | 712                             | 684                             | Mg               |
| propellant consumption pri       | 294.7                   | 626.8                           | 602.3                           | Mg               |
| propellant consumption sec       | 241.                    | -                               | -                               | Mg               |
| total propellant mass            | 535.8                   | 626.8                           | 602.3                           | Mg               |
| mode1 consumption propellant     | 398.                    | 627                             | 602                             | Mg               |
| mode2 consumption propellant     | 138.                    | -                               | -                               | Mg               |
| total engine mass                | 11.4                    | 15.2                            | 13.4                            | Mg               |
| reentry mass                     | 13.6                    | 15.0                            | 14.4                            | Mg               |
| payload fairing mass             | 2.6                     | 2.6                             | 2.6                             | Mg               |
| effective net mass               | 58.8                    | 68.8                            | 65.1                            | Mg               |
| structure mass                   | 32.7                    | 37.1                            | 35.9                            | Mg               |
| all turbo-machinery efficiencies | .75                     | .75                             | .75                             |                  |
| GG-c*-efficiency                 | .98                     | .98                             | .98                             |                  |
| nozzle exit diameter             | 2.06                    | 1.60                            | 1.57                            | m                |
| engine length                    | 3.5                     | 2.8                             | 2.8                             | m                |
| nozzle length                    | 2.73                    | 2.15                            | 2.10                            | m                |
| nozzle exit pressure             | 35000                   | 30000                           | 30000                           | N/m <sup>2</sup> |
| total Delta v                    | 9211                    | 9298                            | 9312                            | m/s              |
| velocity capability mode 1       | 4519                    | 9298                            | 9312                            | m/s              |
| velocity capability mode 2       | 4702                    | -                               | -                               | m/s              |

Table 4: Summary system data of the optimized cycle candidates

| variable                     | dual-<br>expander cycle | full-flow<br>staged comb. cycle | fuel-rich<br>staged comb. cycle | unit |
|------------------------------|-------------------------|---------------------------------|---------------------------------|------|
| structure mass               | 32.7                    | 37.1                            | 35.9                            | Mg   |
| tank mass                    | 18.9                    | 22.4                            | 21.4                            | Mg   |
| structural frame             | 6.3                     | 6.6                             | 6.5                             | Mg   |
| pressurization system mass   | .79                     | .92                             | .88                             | Mg   |
| ox tank mass                 | 8.3                     | 9.9                             | 9.5                             | Mg   |
| fuel tank mass               | 10.6                    | 12.5                            | 12.0                            | Mg   |
| fuel tank hight              | 22                      | 25                              | 24                              | m    |
| oxidizer tank hight          | 10.36                   | 11.81                           | 11.42                           | m    |
| total engine mass            | 11.4                    | 15.2                            | 13.4                            | M    |
| thrust chamber assembly mass | 839                     | 516                             | 508                             | kg   |
| control-, turbopump mass     | 1410                    | 1034                            | 833                             | kg   |
| thrust chamber mass          | 700                     | 261                             | 248                             | kg   |
| miscellaneous engine         | 589                     | 347                             | 334                             | kg   |
| nozzle mass                  | 138                     | 255                             | 260                             | kg   |
| GG-mass                      | 200                     | 264                             | 84                              | kg   |
| turbo pump system mass       | 865                     | 200                             | 443                             | kg   |
| engine valves mass           | 316                     | 125                             | 195                             | kg   |

Table 5: Summary of structure and engine subsystem masses

- [8] R. Beichel, C. J. O'Brian, J. P. Taylor, *Space Transport Propulsion Application - A Development Challenge*, IAF-89-224, 1989
- [9] D. O. Stanley, W. C. Engelund, R. Lepsch, *Propulsion System Requirements for Reusable SSTO Rocket Vehicles*, AIAA-92-3504, 1992
- [10] G. Hagemann, D. Manski, G. Krülle, *Dual-Expander Engine Flowfield Simulations*, AIAA-95-3135, 1995
- [11] D. Manski, G. Hagemann, *Influence of Rocket Design Parameters on Engine Nozzle Efficiencies*, AIAA-94-2756, 1994
- [12] D. Manski, *Effects of Engine Cycle Type on Payload Delivery of the Future European Launchers*, IAF 85-127, 1985
- [13] D. Manski, H. Taniguchi, H. Saßnick, *Comparative Analysis of the Vulcan and the LE-7 Engines Applied in Ariane 5 and H-II Launchers*, 16th International Symposium on Space Technology and Science, Sapporo, Japan, May 1988
- [14] D. Manski, *Analysis and Optimization of Small Space Shuttle Propulsion Platforms*, ESA-TT-901, English version of DFVLR-FB-84-28 European Space Agency, 1985
- [15] D. Manski, J. A. Martin, *Optimization of the Propulsion Cycles for Advanced Shuttles - Part 1: Propulsion Mass Model Methodology*, AIAA-89-2279, 1989
- [16] D. Manski, J. A. Martin, *Optimization of the Propulsion Cycles for Advanced Shuttles - Part 2: Performance Model Methodology*, AIAA-90-2436, 1990
- [17] S. Gordon, B.J. McBride, *Computer Program for Calculation of Complex Chemical Equilibrium Compositions, Rocket Performance, ...*, NASA-SP-273, NASA Lewis Research Center, Cleveland, Ohio, 1976.
- [18] G. R. Nickerson, L. D. Dang, D. E. Coats, *Two Dimensional Reference Computer Program*, NAS 8-35931, Marshall Space Flight Center, 1985
- [19] D. E. Koelle, W. Kleinau, *The Single-Stage Reusable Ballistic Launcher Concept*, IAF-86-122, 1986
- [20] R. K. Weegar, *Engine/Vehicle Integration for Vertical Takeoff and Landing SSTO Vehicles*, IAF-92-065, 1992
- [21] G. L. Bauer, D. E. Cornick, R. Stevenson, *Capabilities and Applications of the Program to Optimize Simulated Trajectories (POST)*, NASA-CR-2770, 1977
- [22] G. Hagemann, *Überschallströmungen reagierender Gase in komplexen Düsenkonfigurationen von Hochleistungs-Raketentriebwerken*, DLR-FB 95-40, DLR Lampoldshausen (in German), 1996